

Beyond Retraining: Training-Free Unknown Class Filtering for Source-Free Open Set Domain Adaptation of Vision–Language Models

Yongguang Li¹, Jindong Li⁴, Qi Wang^{1,2}, QianLi Xing³, Runliang Niu¹, Shengsheng Wang³, Menglin Yang⁴

¹School of Artificial Intelligence, Jilin University,

²Engineering Research Center of Knowledge-Driven Human-Machine Intelligence, Ministry of Education, China

³College of Computer Science and Technology, Jilin University, Changchun, Jilin, 130012, China.

⁴The Hong Kong University of Science and Technology (Guangzhou)

^{1,2,3} {ygli25, niurl19}@mails.jlu.edu.cn, {qiwang, qianlixing, wss}@jlu.edu.cn

⁴jli839@connect.hkust-gz.edu.cn, menglin.yang@outlook.com

Abstract

Vision-language models (VLMs) have gained widespread attention for their strong zero-shot capabilities across numerous downstream tasks. However, these models assume that each test image’s class label is drawn from a predefined label set and lack a reliable mechanism to reject samples from emerging unknown classes when only unlabeled data are available. To address this gap, open-set domain adaptation methods re-train models to push potential unknowns away from known clusters. Yet, some unknown samples remain stably anchored to specific known classes in the VLM feature space due to semantic relevance, which is termed as *Semantic Affinity Anchoring (SAA)*. Forcibly repelling these samples unavoidably distorts the native geometry of VLMs and degrades performance. Meanwhile, existing score-based unknown detectors use simplistic thresholds and suffer from threshold sensitivity, resulting in sub-optimal performance. To address aforementioned issues, we propose VLM-OpenXpert, which comprises two training-free, plug-and-play inference modules. SUFF performs SVD on high-confidence unknowns to extract a low-rank “unknown subspace”. Each sample’s projection onto this subspace is weighted and softly removed from its feature, suppressing unknown components while preserving semantics. BGAT corrects score skewness via a Box–Cox transform, then fits a bimodal Gaussian mixture to adaptively estimate the optimal threshold balancing known-class recognition and unknown-class rejection. Experiments on 9 benchmarks and three backbones (CLIP, SigLIP, ALIGN) under source-free OSDA settings show that our training-free pipeline matches or outperforms retraining-heavy state-of-the-art methods, establishing a powerful lightweight inference calibration paradigm for open-set VLM deployment.

Introduction

Recent advances in large-scale vision-language models (VLMs) such as CLIP (Radford et al. 2021) have demonstrated powerful zero-shot capabilities across diverse downstream tasks without task-specific fine-tuning, making them foundational for real-world applications (Zhang et al. 2024). However, such zero-shot predictions inherently assume a closed-world scenario, where test samples must belong to a predefined label space. This assumption is frequently violated as unlabeled classes inevitably emerge in real-world scenarios (Yu, Irie, and Aizawa 2025). Misclassifying these

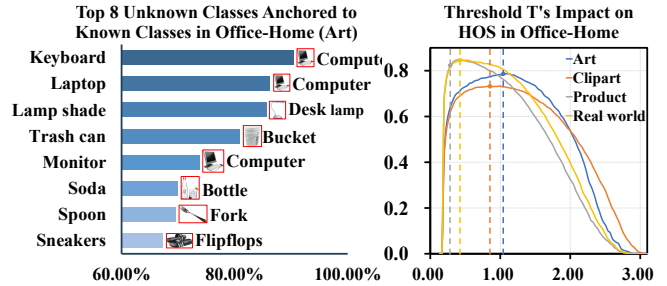


Figure 1: Analysis of CLIP on Office-Home. Left: top-8 unknown classes with the highest anchor rates and their anchored known classes. Right: HOS (%) on four domains versus threshold; the dashed line marks the optimum.

unknown samples as known classes can lead to severe consequences. For instance, autonomous driving systems may misclassify unseen construction machinery as normal vehicles, posing serious safety hazards (Yang et al. 2024). Moreover, real-world deployments typically lack labeled data and involve significant domain shifts, presenting critical challenges for enhancing unknown-class rejection in VLMs.

Against this backdrop, models must retain discriminative power on known classes while reliably rejecting unknown samples using only unlabeled target data. This challenge has given rise to Open-Set Unsupervised Domain Adaptation (OSDA) and its variant, Source-Free OSDA (SF-OSDA) (Fang et al. 2020). Conventional single-modal OSDA methods jointly train on labeled source and unlabeled target data to transfer knowledge and enhance unknown-class detection. The general idea of such methods is to enforce a repulsion loss that pushes potential unknown samples away from known-class clusters (Liu et al. 2019). In contrast, SF-OSDA dispenses with source data at adaptation time, relying solely on a source-pretrained model while still applying the same separation objective (Wan et al. 2024). In the VLM era, many works have directly transplanted this “retraining + separation” paradigm into vision–language settings by using VLM backbones, aiming to establish clear decision boundaries between known and un-

known classes (Liang et al. 2024; Min et al. 2023).

However, this paradigm implicitly relies on the global separability assumption, that unknown classes should be semantically distant from all known classes. Due to inherent semantic affinity, many unknown classes naturally anchor to specific known-class clusters. We term this phenomenon as *Semantic Affinity Anchoring (SAA)*. For example, in Office-Home (Venkateswara et al. 2017), nearly all samples of the unknown class “keyboard” fall into the known “computer” cluster (Figure 1(left)), and over 50% of unknown classes exhibit SAA in CLIP. As SAA reflects the true semantic relationships captured by vision–language pretraining, naively pushing anchored samples away risks distorting the model’s semantic structure and harming performance. In addition to the geometric mismatch, VLM-based unknown sample detection also suffers from threshold sensitivity issue caused by existing score-based strategies. As shown in Figure 1(right), optimal thresholds vary significantly across datasets. Prior approaches often adopt simplistic strategies such as fixed values (Yu, Irie, and Aizawa 2025), mean scores (Bucci, Loghmani, and Tommasi 2020), k-means clustering (Wan et al. 2024), or heuristic rules, which fail to model score distributions effectively and lead to suboptimal performance.

To address such issues, we propose VLM-OpenXpert, a training-free and label-free source-free OSDA framework of vision–language models, featuring two plug-and-play modules. Specifically, the first module, SUFF (SVD-Based Unknown-Class Feature Filtering), which adopts a directional filtering strategy instead of global repulsion. It begins by selecting high-confidence unknown samples using an uncertainty-based criterion, explicitly including those hard-to-detect cases affected by Semantic Affinity Anchoring (SAA). Then, it performs SVD (Eckart and Young 1936) on the centralized features of these samples to construct a low-rank subspace, where unknowns exhibit higher projection energy than knowns. Finally, all samples are softly attenuated based on their projection in this subspace, effectively suppressing unknown-class features while preserving the semantic geometry of the model and mitigating the effects of SAA.

Next, we propose BGAT (Box-Cox GMM-Based Adaptive Thresholding) to replace brittle fixed or heuristic thresholds. BGAT first applies a Box-Cox transformation on confidence scores to stabilize scale and skewness, then fits a bimodal Gaussian mixture in the transformed space. The midpoint between the two modes yields a near-optimal, data-adaptive threshold. These two modules augment VLMs with reliable open-set detection capabilities at inference time with minimal computational overhead and without requiring any labeled samples or retraining. Experimental results demonstrate that our VLM-OpenXpert, despite being entirely training-free, outperforms representative training-intensive OSDA methods. Also, it can serve as a plug-and-play enhancement to boost the performance of existing trainable Source-free OSDA methods. **Our main contributions are summarized as follows:**

- We identify and validate *Semantic Affinity Anchoring (SAA)* phenomenon, where unknown samples being se-

mantically attracted to known classes. We further show that excessively pushing unknowns away from knowns can distort VLM’s inherently generalized feature space, thereby degrading its performance.

- We propose SUFF, a training-free and plug-and-play module that suppresses unknown-class features via selective filtering, alleviating SAA while preserving VLM semantic geometry. Also, we introduce BGAT, a lightweight adaptive thresholding strategy that estimates near-optimal thresholds, enhancing the discriminative ability of VLM on identifying known classes while reliably rejecting unknown samples.
- Experiments on 9 benchmarks and 3 VLM backbones (e.g., CLIP, SigLIP, ALIGN) show that our training-free method matches or outperforms training-heavy representative OSDA methods, establishing a strong training-free baseline for VLM-based open-set domain adaptation.

Related Work

Vision-language Models. Vision–Language Models (VLMs) (Zhang et al. 2024) learn a shared embedding space for images and texts by contrastively aligning large-scale image–caption pairs, enabling simple image–text similarity to power a wide range of downstream tasks without task-specific heads. Representative models such as CLIP, SigLIP, and ALIGN normally adopt a twin-tower architecture with separate vision and text encoders. Such models are trained on massive web-scale datasets and support zero-shot inference via promptable text queries. While this design offers strong cross-task generalization, it lacks a built-in mechanism to reject unseen classes at test time (Wang et al. 2023). To address this limitation, we propose an inference-time calibration procedure that can be seamlessly integrated into any frozen VLM. Our method requires no labels or additional training and equips the model with robust open-set recognition capability, enabling reliable rejection of unknown samples during deployment.

Unsupervised Open-Set Domain Adaptation. OSDA (Panareda Busto and Gall 2017; Li et al. 2025) aims to mitigate the decline in model performance caused by distribution discrepancies between the source and target domains, while assuming that the target domain contains unknown categories absent in the source domain. Traditional OSDA methods (Liu et al. 2019; Bucci, Loghmani, and Tommasi 2020) typically rely on training with both source and target domain data concurrently. However, practical applications may restrict direct access to source domain data during target domain training due to privacy concerns, thereby motivating the development of Source-Free Unsupervised Domain Adaptation (SF-OSDA) (Luo et al. 2023; Qu et al. 2024). Most existing SF-OSDA (Luo et al. 2023; Qu et al. 2024) approaches substitute source domain samples with models pre-trained on the source domain for target domain training. In recent years, capitalizing on CLIP’s remarkable zero-shot transfer capabilities, some SF-OSDA methods have begun to integrate CLIP with a set of known class names to train directly on unlabeled target domain data (Min et al. 2023; Liang et al. 2024). This paper

specifically addresses this scenario by proposing a method that requires no training.

Methodology

Given an unlabeled target dataset $D_t = \{x_i^t\}_{i=1}^{N_t}$ and a set of known categories $L_t = \{l_c\}_{c=1}^C$, where l_c represents the category name of the c -th class, some samples in D_t belong to L_t , while others do not. Our goal is to perform inference on D_t by assigning samples belonging to L_t to their respective known classes and classifying the rest as an unknown class ($C+1$). The model’s performance is evaluated on D_t .

As shown in Figure 2, VLM-OpenXpert uses a frozen VLM backbone for zero-shot inference to produce known-class predictions and compute per-sample scores. It then applies BGAT to estimate a threshold for identifying representative samples to construct the SUFF module, suppresses unknown-class features via SUFF, recomputes scores, and uses BGAT again to determine the threshold for final detection of unknown-class samples.

Box-Cox GMM-Based Adaptive Thresholding (BGAT) Module

Traditional open-set domain adaptation methods typically employ fixed thresholds (e.g., Max/2) (Yu, Irie, and Aizawa 2025) or global means (Bucci, Loghmani, and Tommasi 2020; Liu et al. 2019) to distinguish unknown-class samples, which lack theoretical foundation and oversimplify real-world distributions. To investigate a more universal and adaptive threshold calibration strategy, motivated by previous work (Jahan and Savakis 2024), we introduce a statistically grounded approach combining Box-Cox transformation (Box and Cox 1964) and Gaussian Mixture Models (GMM) (Bishop and Nasrabadi 2006).

Specifically, as shown in Figure 2, given an unlabeled target dataset D_t and a set of known class names $L_t = \{l_1, l_2, \dots, l_C\}$, we perform zero-shot classification on all samples in D_t using a VLM (e.g., CLIP). The classification probabilities for known classes and the detection of unknown samples are computed as follows:

$$\hat{y}_{i,c} = \frac{\exp(\cos(X_{all}[i], X_{text}[c])/t)}{\sum_{c'=1}^C \exp(\cos(X_{all}[i], X_{text}[c'])/t)}, \quad (1)$$

$$\text{Pred}(x_i) = \begin{cases} C + 1, & \text{if Score}(\hat{y}_i) > T^*, \\ \arg \max_c \hat{y}_{i,c}, & \text{otherwise.} \end{cases} \quad (2)$$

In particular, we define:

$$X_{all} = \{E(x_i) \mid x_i \in D_t\}, \quad X_{text} = \{G(p(l_c)) \mid l_c \in L_t\}, \quad (3)$$

where E denotes the image encoder, G denotes the text encoder, and $p(l_c)$ is the class description sentence with the default prompt “a photo of a”. The threshold is denoted by T^* , and we adopt entropy as the default sample score:

$$S(x_i) = H(\hat{y}_i) = - \sum_{c=1}^C \hat{y}_{i,c} \log(\hat{y}_{i,c}). \quad (4)$$

We assume that the score distributions for known-class and unknown-class samples follow Gaussian distributions with different means and variances. Under the common assumption of symmetric costs and comparable priors, the optimal threshold T^* admits the well-known closed form given by the intersection of the two densities (see Theorem 1 in Appendix). However, there are two issues in practical datasets that need to be addressed:

(i) *Distribution Skewness*: Taking the entropy of the samples as an example, the entropy of known classes is concentrated near 0 due to the high certainty of most known-class samples. This results in a significant left skew in distribution, violating the assumption of a Gaussian distribution; (ii) *Error in GMM Estimation*: During the GMM estimation process, errors arise, particularly when the entropy of the samples is highly concentrated, the variance estimation for known classes becomes notably inaccurate, significantly reducing the accuracy of intersection points.

Addressing Issue (i): We apply the Box–Cox (Box and Cox 1964) transformation; to ensure positivity, add a tiny $\epsilon > 0$ to the scores (still denoted S_i). The transform is:

$$S_i^{(\lambda)} = \begin{cases} \frac{S_i^\lambda - 1}{\lambda}, & \lambda \neq 0, \\ \log S_i, & \lambda = 0. \end{cases} \quad (5)$$

where the optimized parameter λ^* is estimated using maximum likelihood (Fisher 1921) as:

$$\lambda^* = \arg \max_{\lambda} \sum_{i=1}^N \log \mathcal{N}(S_i^{(\lambda)}; \mu_\lambda, \sigma_\lambda^2) + (\lambda-1) \sum_{i=1}^N \log S_i. \quad (6)$$

Since this data transformation is monotonically increasing, it does not alter the relative ordering of the sample scores. However, it can alleviate the issue of sample scores being too close to known classes, thereby improving the accuracy of mean and variance estimation.

Addressing Issue (ii): After Box–Cox transformation, we fit a two-component GMM to $\{S_i^{(\lambda^*)}\}$ as:

$$p(S^{(\lambda^*)}) = \pi_1 \mathcal{N}(\mu_1, \sigma_1^2) + \pi_2 \mathcal{N}(\mu_2, \sigma_2^2), \quad (7)$$

Parameters $\{\pi_k, \mu_k, \sigma_k\}_{k=1}^2$ are estimated via EM (Dempster, Laird, and Rubin 1977) and sorted as $(\mu_{\text{low}}, \sigma_{\text{known}})$, $(\mu_{\text{high}}, \sigma_{\text{unk}})$. However, the GMM estimation may introduce errors, particularly the underestimation of the known-class variance σ_{known} . Since the intersection point is highly sensitive to the variance (as shown in Theorem 2 of Appendix), it may not be the optimal choice in practice.

To address this issue, we adopt a compromise approach by selecting the midpoint of the means, $T_{\text{trans}}^* = \frac{\mu_{\text{known}} + \mu_{\text{unk}}}{2}$, as the threshold. This choice is motivated by the fact that the mean estimated by GMM is less sensitive to errors than the variance, and using the midpoint can enhance the robustness of the threshold. Finally, the optimal threshold T^* is derived via inverse Box-Cox transformation as:

$$T^* = \begin{cases} (\lambda^* T_{\text{trans}}^* + 1)^{1/\lambda^*}, & \lambda^* \neq 0, \\ \exp(T_{\text{trans}}^*), & \lambda^* = 0. \end{cases} \quad (8)$$

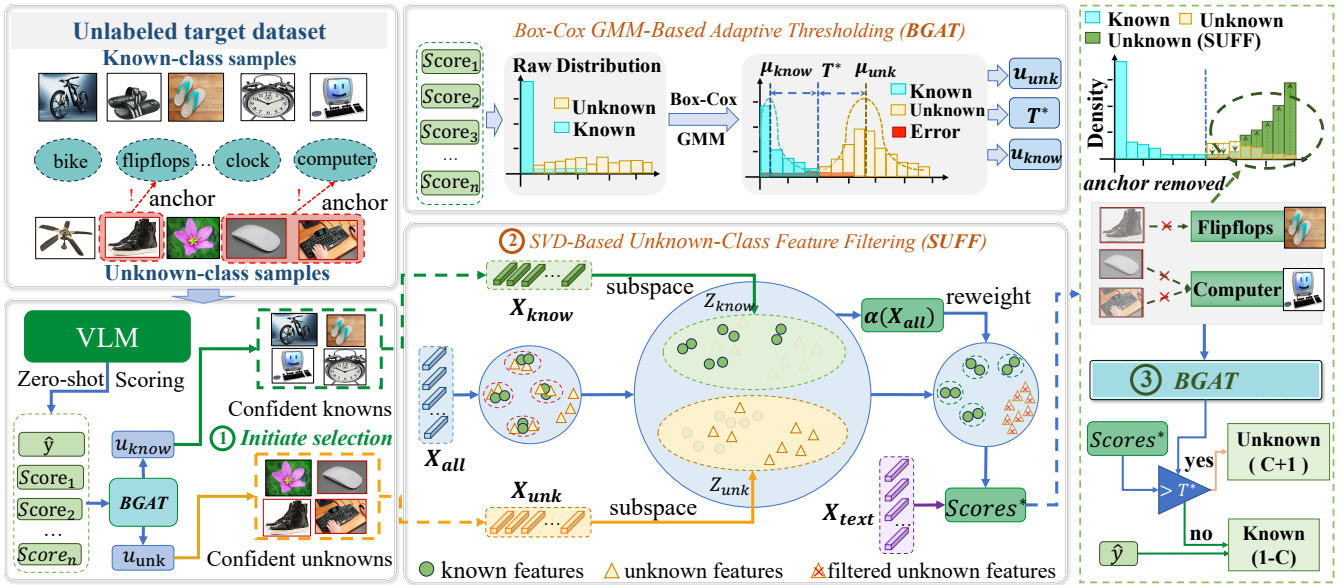


Figure 2: Overview of VLM-OpenXpert, which performs lightweight, training-free inference on unlabeled target data via entropy-based scoring, unknown-class feature filtering (SUFF), and adaptive thresholding (BGAT).

In addition, the estimated means ($\mu_{\text{know}}, \mu_{\text{unk}}$) of the known and unknown classes also need to be transformed back to the space before the Box-Cox transformation.

SVD-Based Unknown-Class Feature Filtering (SUFF) Module

Although the BGAT module estimates the optimal threshold T^* , the SAA phenomenon still causes some unknown-class samples to have low entropy and be misclassified as known-class samples. To resolve this, we propose an SVD-based Unknown Feature Filtering Module (SUFF), which filters out unknown-class features from X_{all} to mitigate the SAA phenomenon.

Specifically, we use the known-class mean μ_{know} , along with the unknown-class mean μ_{unk} and threshold T^* , both estimated by the BGAT module from VLM zero-shot scores, to filter high-confidence known- and unknown-class sample features. We filter samples with entropy less than or equal to $\frac{\mu_{\text{know}} + T^*}{2}$, forming the high-confidence known-class sample feature set $X_{\text{know}} \in \mathbb{R}^{N_{\text{know}} \times D}$; and we filter samples with entropy greater than $\frac{\mu_{\text{unk}} + T^*}{2}$, forming the high-confidence unknown-class sample feature set $X_{\text{unk}} \in \mathbb{R}^{N_{\text{unk}} \times D}$.

Next, we perform SVD on both known-class and unknown-class feature sets to construct their principal component subspaces as:

$$X_{\text{know}} = U_{\text{know}} \Sigma_{\text{know}} V_{\text{know}}^{\top}, \quad (9)$$

$$X_{\text{unk}} = U_{\text{unk}} \Sigma_{\text{unk}} V_{\text{unk}}^{\top}, \quad (10)$$

where $\Sigma_{\text{know}} = \text{diag}(\sigma_1^{\text{know}}, \dots, \sigma_r^{\text{know}})$ and $\Sigma_{\text{unk}} = \text{diag}(\sigma_1^{\text{unk}}, \dots, \sigma_r^{\text{unk}})$ are the singular value matrices. $V_{\text{know}} \in \mathbb{R}^{r \times D}$ and $V_{\text{unk}} \in \mathbb{R}^{r \times D}$ are the right singular matrices. The smallest dimension k is selected such that the cumulative variance contribution satisfies the following:

$$\min k \quad \text{s.t.} \quad \frac{\sum_{i=1}^k (\sigma_i)^2}{\sum_{j=1}^r (\sigma_j)^2} \geq \tau. \quad (11)$$

We retain the top k principal components to construct the projection matrices $W_{\text{know}} = V_{\text{know}}[:, k, :]^{\top}$ and $W_{\text{unk}} = V_{\text{unk}}[:, k, :]^{\top}$. Then, we project all sample features $X_{\text{all}} \in \mathbb{R}^{N \times D}$ into the constructed known class space Z_{know} and unknown class space Z_{unk} as follows:

$$X_{\text{all}}^{\text{know}} = Z_{\text{know}}(X_{\text{all}}) = X_{\text{all}} W_{\text{know}} W_{\text{know}}^{\top}, \quad (12)$$

$$X_{\text{all}}^{\text{unk}} = Z_{\text{unk}}(X_{\text{all}}) = X_{\text{all}} W_{\text{unk}} W_{\text{unk}}^{\top}. \quad (13)$$

Next, we analyze the proportion $\alpha(X_{\text{all}})$ of unknown class features in the samples based on the similarity $S(x_{\text{all}})$ before and after normalizing the sample feature mapping:

$$s_{\text{know}}(X_{\text{all}}) = \frac{X_{\text{all}} \cdot X_{\text{all}}^{\text{know}}}{\|X_{\text{all}}\| \|X_{\text{all}}^{\text{know}}\|}, \quad (14)$$

$$s_{\text{unk}}(X_{\text{all}}) = \frac{X_{\text{all}} \cdot X_{\text{all}}^{\text{unk}}}{\|X_{\text{all}}\| \|X_{\text{all}}^{\text{unk}}\|}, \quad (15)$$

$$\alpha(X_{\text{all}}) = \frac{\exp(s_{\text{unk}}(X_{\text{all}})/t)}{\exp(s_{\text{know}}(X_{\text{all}})/t) + \exp(s_{\text{unk}}(X_{\text{all}})/t)}, \quad (16)$$

where t is temperature coefficient. t is set to 1.0 by default and it controls the smoothness of probability distribution.

To remove the unknown-class features from the sample features, we perform a weighted subtraction operation:

$$X_{\text{all}}^* = X_{\text{all}} - \alpha(X_{\text{all}}) X_{\text{all}}^{\text{unk}}, \quad (17)$$

Finally, we recompute sample scores using the filtered features X_{all}^* and X_{text} , and re-estimate the threshold T^* via BGAT. Samples scoring above T^* are marked as unknown, while others retain their original predictions from Eq. 1, preserving known-class recognition and mitigating filtering-induced errors.

method	E	VLM	TF	OfficeHome												VisDA	
				C	P	R	A	P	R	A	C	R	A	C	P	AVG	Syn
				A			C			P			R				Real
OSDA (trains jointly on labeled source data and unlabeled target data)																	
USD	RN	×	×	60.1	62.6	67.8	61.1	56.3	59.1	70.0	65.2	71.1	76.3	68.9	56.3	64.6	69.4
OSMDA-CLIP	Vit-B-32	✓	×	74.1	74.7	76.6	71.9	69.7	70.4	81.9	82.2	81.8	83.8	84.0	69.7	76.7	83.4
UniOT-CLIP	Vit-B-16	✓	×	79.2	71.8	77.1	77.8	72.3	76.0	83.3	83.1	87.3	86.3	84.1	84.7	80.3	-
GLC-CLIP	Vit-B-16	✓	×	55.5	52.1	69.0	72.1	65.9	71.3	79.7	81.3	83.9	83.3	77.9	65.9	71.5	83.4
SF-OSDA (uses a model trained on labeled source data and performs unsupervised training on unlabeled target data)																	
LEAD	RN	×	×	61.0	65.5	64.8	60.7	59.8	57.7	70.8	68.6	75.8	76.5	70.8	59.8	66.0	74.2
DTDE	RN	×	×	-	-	-	-	-	-	-	-	-	-	-	-	70.3	80.4
(Co-learn++)-CLIP	RN	✓	×	60.4	56.0	64.0	54.9	51.0	58.8	77.6	72.7	83.6	78.4	75.9	51.0	65.4	-
COSDA	RN	×	×	65.0	67.8	70.3	70.5	63.7	64.1	74.9	72.2	79.1	79.9	76.1	63.7	70.6	-
UPUK	RN	×	×	66.4	67.6	67.8	55.8	55.1	59.4	76.7	73.1	74.4	78.4	77.6	55.1	67.3	72.3
COCA-CLIP	Vit-B-16	✓	×	79.7	79.6	80.0	75.6	74.5	75.7	84.5	84.3	84.4	82.5	82.5	74.5	79.8	86.3
COSDA-CLIP	Vit-B-32	✓	×	-	-	-	-	-	-	-	-	-	-	-	-	-	78.4
DIFO-CLIP	Vit-B-32	✓	×	68.2	67.2	71.9	64.5	62.1	65.3	86.2	79.3	84.4	87.9	86.1	62.1	73.8	-
Target-only Adaptation (adapts directly on the unlabeled target domain; notably, only our method performs inference without any training)																	
UOTA-CLIP	Vit-B-32	✓	×	75.9			75.1			84.2			86.2			80.4	85.3
UEO-CLIP	Vit-B-16	✓	×	72.1			71.1			79.5			79.5			75.6	82.6
ours-CLIP	RN	✓	✓	73.5			61.9			81.9			81.6			74.7	85.1
ours-CLIP	Vit-B-32	✓	✓	75.1			72.8			85.1			87.2			80.0	87.6
ours-CLIP	Vit-B-16	✓	✓	78.2			74.0			86.8			85.7			81.2	89.0
ours-SigLIP	Vit-B-16	✓	✓	85.8			<u>82.9</u>			<u>90.0</u>			<u>89.2</u>			<u>87.0</u>	<u>88.3</u>
ours-ALIGN	EfficientNet-B7	✓	✓	<u>85.0</u>			83.2			90.9			91.3			87.6	87.3

Table 1: HOS (%) on Office-Home and VisDA-2017. Bold denotes the best results and underline denotes the second best. “-CLIP”, “-SigLIP”, and “-ALIGN” represent using the respective VLM backbone. (E: Image Encoder; SF-S: Source-Free; TF: Training-Free).

Experiments

Experimental Settings

Datasets. We evaluate our method under the SF-OSDA experimental setting on three representative benchmark datasets: Office-Home (Venkateswara et al. 2017) (65 categories, 4 domains), VisDA-2017 (Peng et al. 2017) (12 categories, synthetic-to-real adaptation), and DomainNet (Peng et al. 2019) (345 categories, 6 domains). To further test the generalization ability of our model, we select 6 datasets from the Visual Task Adaptation Benchmark (VTAB-6).

Baselines. We select three categories of baseline methods for comparison: **OSDA/SF-OSDA methods** jointly train on source data (or a source-trained model) and unlabeled target data, including USD (Jahan and Savakis 2024), LEAD (Qu et al. 2024), DIFO (Tang et al. 2024), OSMDA (Liu et al. 2025), UniOT (Chang et al. 2022), GLC (Qu et al. 2023), COCA (Liu and Zhou 2024), DTDE (Yu et al. 2025), Co-learn++ (Zhang, Shen, and Foo 2025), COSDA (Wang et al. 2025), UPUK (Wan et al. 2024); **Unsupervised target-only adaptation methods** such as UOTA (Min et al. 2023) and UEO (Liang et al. 2024), which perform training and unknown class detection directly on the target domain; **CLIP-based zero-shot OOD methods** using Maximum Concept Matching (MCM) (Ming et al. 2022).

Implementation Details. We evaluate on three VLM backbones—CLIP (Radford et al. 2021), SigLIP (Zhai et al. 2023), and ALIGN (Jia et al. 2021). Image encoders follow the table headers; when unspecified, we default to ViT-B/16 (Han et al. 2022) for CLIP and SigLIP, and

Method	E	VTAB-6	DomainNet	AVG
MCM-CLIP	ViT-L/14	59.9	67.8	63.9
MCM-SigLIP	ViT-B/16	66.3	66.5	66.4
MCM-ALIGN	EfficientNet-B7	59.3	66.6	62.9
UOTA-CLIP	ViT-L/14	-	71.1	-
UEO-CLIP	ViT-L/14	57	69.6	63.3
ours-CLIP	ViT-L/14	<u>65.4</u>	72.9	<u>69.1</u>
ours-SigLIP	ViT-B/16	70.2	<u>70.8</u>	70.5
ours-ALIGN	EfficientNet-B7	62.2	66.9	64.5

Table 2: HOS (%) on DomainNet and six visual task adaptation datasets.

EfficientNet-B7 (Tan and Le 2019) for ALIGN. Unless otherwise noted, we set $\tau = 0.8$ and use a batch size of 32. See Appendix for more details.

Overall Performance

As shown in Table 1 and Table 2, our training-free approach surpasses previous OSDA, SF-OSDA, and target-only adaptation methods. Using the same backbone on Office-Home, it outperforms GLC, DIFO, and UEO by 9.7%, 7.4%, and 5.6%, respectively. Compared with the state-of-the-art UOTA, it achieves gains of 3.7% on VisDA-2017 and 1.8% on DomainNet, while matching UOTA on Office-Home. These results confirm the effectiveness of our method and show that an efficient, training-free inference strategy can unlock the inherent open-set zero-shot capability of VLMs

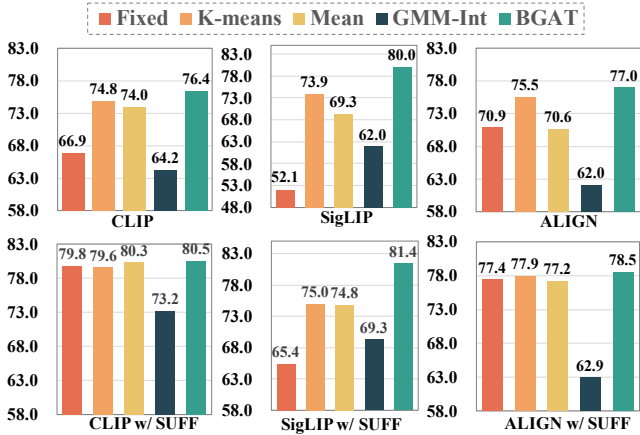


Figure 3: HOS(%) performance variation under different thresholding methods.

on unlabeled target data. Moreover, our approach consistently outperforms MCM on three different VLM backbones across all six Visual Task Adaptation benchmarks, demonstrating the robust improvements in unknown-class detection. Notably, our method adds only 2.5% inference time compared to direct zero-shot use of VLMs, while being tens of times faster than conventional training-intensive methods. See Appendices and for more details.

Ablation Study

Analysis of the SAA Phenomenon. To quantitatively validate how much unknown samples concentrate around a single known class, we propose the Anchor Rate at 1 (e.g., AR@1) metric, which is defined as the fraction of unknown classes whose strongest semantic affinity is with one known class (e.g., range 0–1). As shown in Table 3, all three VLMs exhibit high AR@1 values (0.46–0.58) on the widely used benchmarks, indicating that about half of unknown classes in these benchmarks anchor to specific known-class clusters, thereby confirming the widespread presence of the SAA phenomenon. See Appendix for detailed analysis.

Effectiveness of SUFF. As shown in Table 3, SUFF reduces AR@1 by 0.23, 0.28, and 0.33 on CLIP, SigLIP, and ALIGN, respectively, directly demonstrating substantial mitigation of semantic affinity anchoring (SAA). This reduction translates into average HOS gains of 7.7%, 6.9%, and 4.3% across all thresholding strategies (Table 4), confirming improved known/unknown separability. Figures 4 and 6 further illustrate SUFF’s dual effect: it separates unknown classes while preserving known-class separability and markedly reduces their clustering around specific known classes. See Appendix for detailed results.

Effectiveness of BGAT. We compare five thresholding strategies across six tasks using three VLMs: a fixed threshold at half the maximum score (Fixed) (Yu, Irie, and Aizawa 2025), the mean of all scores (Mean) (Bucci, Loghmani, and Tommasi 2020), k-means clustering (K-Means) (Liang, Hu, and Feng 2020), the intersection point of two Gaussian densities (GMM-Int) (He, Wang, and Zhang 2025), and our pro-

Method	VTAB-6	Office-Home	VisDA-2017	AVG↓
CLIP	0.53	0.53	0.33	0.46
CLIP w/ SUFF	0.44	0.24	0.00	0.23(↓ 0.23)
SigLIP	0.56	0.67	0.50	0.58
SigLIP w/ SUFF	0.32	0.24	0.33	0.30(↓ 0.28)
ALIGN	0.57	0.54	0.50	0.54
ALIGN w/ SUFF	0.32	0.14	0.17	0.21(↓ 0.33)

Table 3: AR@1 on VTAB-6, Office-Home and VisDA-2017 for baseline vs. SUFF-augmented models (↓ lower is better).

VLM	w/ SUFF	Fixed	k-means	BGAT	AVG
CLIP	×	66.9	74.0	76.4	72.4
	✓	79.8(+12.9%)	80.3(+6.2%)	80.5(+4.1%)	80.1(+7.7%)
SigLIP	×	52.1	69.3	80.0	67.1
	✓	65.4(+13.3%)	74.8(+5.5%)	81.4(+1.4%)	73.9(+6.9%)
ALIGN	×	70.9	70.6	77.0	72.8
	✓	77.4(+6.5%)	77.2(+6.6%)	78.5(+1.5%)	77.7(+4.3%)

Table 4: HOS(%) before vs. after SUFF across different VLM backbones and threshold strategies.

posed BGAT method. As shown in Figure 3, BGAT consistently achieves the best performance across all VLMs, both on raw features and SUFF-enhanced features, demonstrating its robustness and adaptability to feature variations. See Appendix refappendix:Ablation-Study for detailed results.

Method	Art	Clipart	Product	Real	AVG
SHOT	58.1	50.8	59.9	62.3	57.8
w/ BGAT	59.2	54.8	65.7	68.8	62.1(+4.3%)
w/ BGAT + SUFF	59.3	55.3	66.5	70.5	62.9(+5.1%)
UEO-CLIP	68.3	63.7	65.6	70.4	67.0
w/ BGAT	72.1	71.1	79.5	80.7	75.9(+8.9%)
w/ BGAT + SUFF	74.8	73.5	83.6	83.3	78.8(+11.8%)

Table 5: HOS (%) for SHOT and UEO-CLIP enhanced with our modules on the four Office-Home subdomains.

Plug-and-Play Validation on UEO and SHOT. Table 5 demonstrates the effectiveness of our proposed BGAT and SUFF modules when integrated into the VLM-based method UEO and the representative single-modal SF-OSDA method SHOT (Liang, Hu, and Feng 2020). As shown in Table 5, adding BGAT improves UEO and SHOT by 8.9% and 4.3% in terms of HOS; with SUFF added, these gains rise to 11.8% and 5.1%. This confirms the generality of our approach across both multimodal and single-modal methods.

Effectiveness of Box-Cox. As shown in Figure 5(a–c), applying the Box–Cox transformation in BGAT consistently improves performance across five tasks and three VLM backbones, confirming its effectiveness in improving threshold estimation and overall accuracy. On average, the three VLMs gain 2.67%, with SigLIP benefiting the most due to its more concentrated known-class scores, which make Box-Cox more effective. See Appendix for more details.

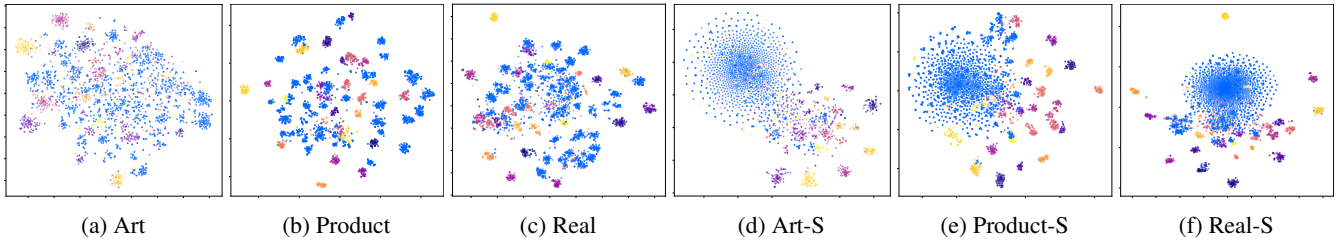


Figure 4: t-SNE Visualizations of four domains in the Office-Home datasets. (a)-(c) represent the raw features obtained from CLIP for target dataset image samples, while (d)-(f) represent the features filtered by the SUFF module. Blue points indicate unknown class samples, and the points in other colors represent different known classes.

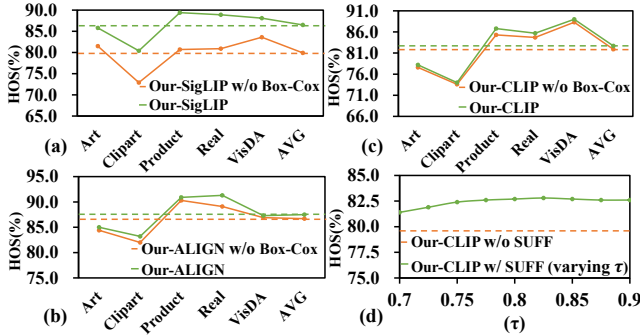


Figure 5: Effect of the Box-Cox transformation and SUFF on HOS (%) for Office-Home and VisDA datasets. Panels (a-c) show the impact of Box-Cox transformation and panel (d) shows the effect of varying τ .

Hyper-parameter Analysis

We analyze the effect of the variance retention ratio (τ) used in subspace construction (Eq. 11). Since the singular value spectrum decays rapidly and then flattens, small τ values may discard useful information, while large τ values tend to retain noise or redundancy. As a result, extreme values offer no meaningful benefit, and we explore a practical range of [0.7, 0.9]. As shown in Figure 5 (d), the average HOS remains consistently stable across five tasks, with a variance of just 0.19 (%)², indicating that model performance is largely insensitive to the choice of τ within this range.

Case Study

Visualization of Semantic Affinity Anchoring. Figure 6 shows heat maps of the anchoring of unknown to known classes (a) before SUFF module and (b) after SUFF module, with anchored unknowns dropping from 18 to 4. This shows SUFF greatly reduces semantic affinity anchoring from unknowns to known classes. The few remaining anchors result from the limits in VLM’s initial sample selection, making it difficult for the unknown-class subspace to cover the feature distribution of these unknown samples. **t-SNE Visualization.** Figure 4 (a-c) shows the original VLM feature distribution, where unknown-class features are mixed with known-class clusters and hard to distinguish. After applying SUFF (Figure 4 (d-f)), unknown features are clearly separated, and the separability among known classes is also pre-

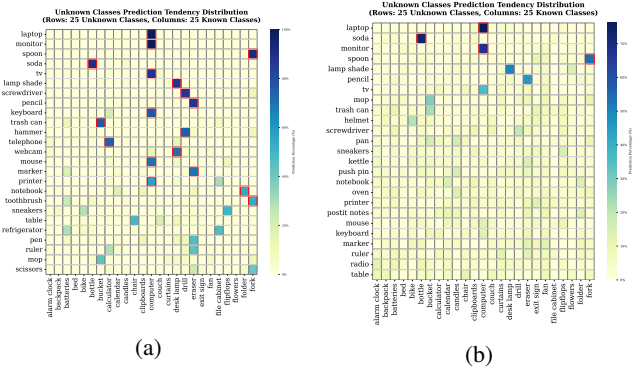


Figure 6: Unknown-class heat map in the Real-World domain of the Office-Home dataset for the ALIGN model: (a) before SUFF processing and (b) after SUFF processing.

served. This confirms that SUFF improves known/unknown discrimination without harming known-class structure.

Conclusion

This work identifies and formally defines *Semantic Affinity Anchoring (SAA)*, a phenomenon common to many benchmark datasets. In SAA, certain unknown-class samples cluster near semantically related known classes in the VLM feature space, which makes them hard to detect. To tackle this problem, we propose VLM-OpenXpert, a completely training-free and label-free inference framework consisting of two plug-and-play modules. Specifically, SUFF filters unknown-class features through soft suppression in a low-rank subspace dominated by unknown-class feature energy, significantly reducing SAA-induced detection failures. BGAT combines a Box-Cox transformation with a bimodal Gaussian mixture model to adaptively estimate an optimal threshold that balances known class recognition and unknown class detection. With these two lightweight inference modules, VLM-OpenXpert surpasses or matches training-intensive state-of-the-art methods on unlabeled target domains, validating its effectiveness and establishing a new design paradigm for unsupervised open-set domain adaptation of vision-language models.

Acknowledgements

This work is supported by the National Natural Science Foundation of China (No.62206107 and No.62406127).

References

- Bishop, C. M.; and Nasrabadi, N. M. 2006. *Pattern recognition and machine learning*, volume 4. Springer.
- Bossard, L.; Guillaumin, M.; and Van Gool, L. 2014. Food-101—mining discriminative components with random forests. In *Computer vision—ECCV 2014: 13th European conference, zurich, Switzerland, September 6–12, 2014, proceedings, part VI 13*, 446–461. Springer.
- Box, G. E.; and Cox, D. R. 1964. An analysis of transformations. *Journal of the Royal Statistical Society Series B: Statistical Methodology*, 26(2): 211–243.
- Bucci, S.; Loghmani, M. R.; and Tommasi, T. 2020. On the effectiveness of image rotation for open set domain adaptation. In *European conference on computer vision*, 422–438. Springer.
- Chang, W.; Shi, Y.; Tuan, H.; and Wang, J. 2022. Unified optimal transport framework for universal domain adaptation. *Advances in Neural Information Processing Systems*, 35: 29512–29524.
- Cimpoi, M.; Maji, S.; Kokkinos, I.; Mohamed, S.; and Vedaldi, A. 2014. Describing textures in the wild. In *Proceedings of the IEEE conference on computer vision and pattern recognition*, 3606–3613.
- Dempster, A. P.; Laird, N. M.; and Rubin, D. B. 1977. Maximum likelihood from incomplete data via the EM algorithm. *Journal of the royal statistical society: series B (methodological)*, 39(1): 1–22.
- Deng, J.; Dong, W.; Socher, R.; Li, L.-J.; Li, K.; and Fei-Fei, L. 2009. Imagenet: A large-scale hierarchical image database. In *2009 IEEE conference on computer vision and pattern recognition*, 248–255. Ieee.
- Eckart, C.; and Young, G. 1936. The approximation of one matrix by another of lower rank. *Psychometrika*, 1(3): 211–218.
- Fang, Z.; Lu, J.; Liu, F.; Xuan, J.; and Zhang, G. 2020. Open set domain adaptation: Theoretical bound and algorithm. *IEEE transactions on neural networks and learning systems*, 32(10): 4309–4322.
- Fisher, R. A. 1921. On the “probable error” of a coefficient of correlation deduced from a small sample. *Metron*, 1: 3–32.
- Han, K.; Wang, Y.; Chen, H.; Chen, X.; Guo, J.; Liu, Z.; Tang, Y.; Xiao, A.; Xu, C.; Xu, Y.; et al. 2022. A survey on vision transformer. *IEEE transactions on pattern analysis and machine intelligence*, 45(1): 87–110.
- He, W.; Wang, Z.; and Zhang, Y. 2025. Target Semantics Clustering via Text Representations for Robust Universal Domain Adaptation. In *Proceedings of the AAAI Conference on Artificial Intelligence*, volume 39, 17132–17140.
- Helber, P.; Bischke, B.; Dengel, A.; and Borth, D. 2019. Eurosat: A novel dataset and deep learning benchmark for land use and land cover classification. *IEEE Journal of Selected Topics in Applied Earth Observations and Remote Sensing*, 12(7): 2217–2226.
- Jahan, C. S.; and Savakis, A. 2024. Unknown sample discovery for source free open set domain adaptation. In *Proceedings of the IEEE/CVF Conference on Computer Vision and Pattern Recognition*, 1067–1076.
- Jia, C.; Yang, Y.; Xia, Y.; Chen, Y.-T.; Parekh, Z.; Pham, H.; Le, Q.; Sung, Y.-H.; Li, Z.; and Duerig, T. 2021. Scaling up visual and vision-language representation learning with noisy text supervision. In *International conference on machine learning*, 4904–4916. PMLR.
- Krause, J.; Stark, M.; Deng, J.; and Fei-Fei, L. 2013. 3d object representations for fine-grained categorization. In *Proceedings of the IEEE international conference on computer vision workshops*, 554–561.
- Li, J.; Li, Y.; Fu, Y.; Liu, J.; Liu, Y.; Yang, M.; and King, I. 2025. CLIP-Powered Domain Generalization and Domain Adaptation: A Comprehensive Survey. *arXiv preprint arXiv:2504.14280*.
- Liang, J.; Hu, D.; and Feng, J. 2020. Do we really need to access the source data? source hypothesis transfer for unsupervised domain adaptation. In *International conference on machine learning*, 6028–6039. PMLR.
- Liang, J.; Sheng, L.; Wang, Z.; He, R.; and Tan, T. 2024. Realistic unsupervised CLIP fine-tuning with universal entropy optimization. In *Proceedings of the 41st International Conference on Machine Learning*, 29667–29681.
- Liu, B.; Xu, Y.; Xu, C.; Xu, X.; and He, S. 2025. Open-set mixed domain adaptation via visual-linguistic focal evolving. *IEEE Transactions on Circuits and Systems for Video Technology*.
- Liu, H.; Cao, Z.; Long, M.; Wang, J.; and Yang, Q. 2019. Separate to adapt: Open set domain adaptation via progressive separation. In *Proceedings of the IEEE/CVF conference on computer vision and pattern recognition*, 2927–2936.
- Liu, X.; and Zhou, Y. 2024. COCA: Classifier-Oriented Calibration via Textual Prototype for Source-Free Universal Domain Adaptation. In *Proceedings of the Asian Conference on Computer Vision*, 1671–1687.
- Luo, Y.; Wang, Z.; Chen, Z.; Huang, Z.; and Baktashmotlagh, M. 2023. Source-free progressive graph learning for open-set domain adaptation. *IEEE Transactions on Pattern Analysis and Machine Intelligence*, 45(9): 11240–11255.
- Min, Y.; Ryoo, K.; Kim, B.; and Kim, T. 2023. UOTA: Unsupervised Open-Set Task Adaptation Using a Vision-Language Foundation Model. In *Workshop on Efficient Systems for Foundation Models@ ICML2023*.
- Ming, Y.; Cai, Z.; Gu, J.; Sun, Y.; Li, W.; and Li, Y. 2022. Delving into out-of-distribution detection with vision-language representations. *Advances in neural information processing systems*, 35: 35087–35102.
- Nilsback, M.-E.; and Zisserman, A. 2008. Automated flower classification over a large number of classes. In *2008 Sixth Indian conference on computer vision, graphics & image processing*, 722–729. IEEE.

- Panareda Busto, P.; and Gall, J. 2017. Open set domain adaptation. In *Proceedings of the IEEE international conference on computer vision*, 754–763.
- Parkhi, O. M.; Vedaldi, A.; Zisserman, A.; and Jawahar, C. 2012. Cats and dogs. In *2012 IEEE conference on computer vision and pattern recognition*, 3498–3505. IEEE.
- Peng, X.; Bai, Q.; Xia, X.; Huang, Z.; Saenko, K.; and Wang, B. 2019. Moment matching for multi-source domain adaptation. In *Proceedings of the IEEE/CVF international conference on computer vision*, 1406–1415.
- Peng, X.; Usman, B.; Kaushik, N.; Hoffman, J.; Wang, D.; and Saenko, K. 2017. Visda: The visual domain adaptation challenge. *arXiv preprint arXiv:1710.06924*.
- Qu, S.; Zou, T.; He, L.; Röhrbein, F.; Knoll, A.; Chen, G.; and Jiang, C. 2024. Lead: Learning decomposition for source-free universal domain adaptation. In *Proceedings of the IEEE/CVF Conference on Computer Vision and Pattern Recognition*, 23334–23343.
- Qu, S.; Zou, T.; Röhrbein, F.; Lu, C.; Chen, G.; Tao, D.; and Jiang, C. 2023. Upcycling models under domain and category shift. In *Proceedings of the IEEE/CVF conference on computer vision and pattern recognition*, 20019–20028.
- Radford, A.; Kim, J. W.; Hallacy, C.; Ramesh, A.; Goh, G.; Agarwal, S.; Sastry, G.; Askell, A.; Mishkin, P.; Clark, J.; et al. 2021. Learning transferable visual models from natural language supervision. In *International conference on machine learning*, 8748–8763. PMLR.
- Tan, M.; and Le, Q. 2019. EfficientNet: Rethinking Model Scaling for Convolutional Neural Networks. In Chaudhuri, K.; and Salakhutdinov, R., eds., *Proceedings of the 36th International Conference on Machine Learning*, volume 97 of *Proceedings of Machine Learning Research*, 6105–6114. PMLR.
- Tang, S.; Su, W.; Ye, M.; and Zhu, X. 2024. Source-free domain adaptation with frozen multimodal foundation model. In *Proceedings of the IEEE/CVF Conference on Computer Vision and Pattern Recognition*, 23711–23720.
- Venkateswara, H.; Eusebio, J.; Chakraborty, S.; and Panchanathan, S. 2017. Deep hashing network for unsupervised domain adaptation. In *Proceedings of the IEEE conference on computer vision and pattern recognition*, 5018–5027.
- Wan, F.; Zhao, H.; Yang, X.; and Deng, C. 2024. Unveiling the unknown: Unleashing the power of unknown to known in open-set source-free domain adaptation. In *Proceedings of the IEEE/CVF Conference on Computer Vision and Pattern Recognition*, 24015–24024.
- Wang, H.; Li, Y.; Yao, H.; and Li, X. 2023. Clipn for zero-shot ood detection: Teaching clip to say no. In *Proceedings of the IEEE/CVF International Conference on Computer Vision*, 1802–1812.
- Wang, W.; Zhou, R.; Wang, J.; Zhou, Y.; Zhu, C.; Tang, R.; Han, B.; and Zhang, N. L. 2025. COSDA: Counterfactual-based Susceptibility Risk Framework for Open-Set Domain Adaptation. In *Forty-second International Conference on Machine Learning*.
- Yang, Z.; Yue, J.; Ghamisi, P.; Zhang, S.; Ma, J.; and Fang, L. 2024. Open set recognition in real world. *International Journal of Computer Vision*, 132(8): 3208–3231.
- Yu, Q.; Irie, G.; and Aizawa, K. 2025. Open-set domain adaptation with visual-language foundation models. *Computer Vision and Image Understanding*, 250: 104230.
- Yu, Z.; Liao, Z.; Li, J.; Chen, Z.; and Zhu, L. 2025. Dynamic Target Distribution Estimation for Source-Free Open-Set Domain Adaptation. In *Proceedings of the AAAI Conference on Artificial Intelligence*, volume 39, 22254–22262.
- Zhai, X.; Mustafa, B.; Kolesnikov, A.; and Beyer, L. 2023. Sigmoid loss for language image pre-training. In *Proceedings of the IEEE/CVF international conference on computer vision*, 11975–11986.
- Zhang, J.; Huang, J.; Jin, S.; and Lu, S. 2024. Vision-language models for vision tasks: A survey. *IEEE transactions on pattern analysis and machine intelligence*, 46(8): 5625–5644.
- Zhang, W.; Shen, L.; and Foo, C.-S. 2025. Source-free domain adaptation guided by vision and vision-language pre-training. *International Journal of Computer Vision*, 133(2): 844–866.
- Zhou, K.; Yang, J.; Loy, C. C.; and Liu, Z. 2022. Learning to prompt for vision-language models. *International Journal of Computer Vision*, 130(9): 2337–2348.

Appendix

Proof

Theorem 1:

Let the known class follow a Gaussian distribution $N(\mu_1, \sigma_1^2)$ and the unknown class follow a Gaussian distribution $N(\mu_2, \sigma_2^2)$, where $\mu_1 < \mu_2$. Define the total classification error area as:

$$E(t) = \int_{-\infty}^t f_2(x)dx + \int_t^{\infty} f_1(x)dx$$

where $f_1(x)$ and $f_2(x)$ denote the probability density functions (PDFs) of the two distributions. Then, the optimal threshold T^* that minimizes $E(t)$ satisfies:

$$f_1(T^*) = f_2(T^*)$$

i.e., T^* is the x-coordinate of the intersection point of the two Gaussian PDFs.

Proof. To find the threshold T^* that minimizes the total classification error $E(t)$, we analyze the structure of the error function as follows:

1. Construction of the Error Function

The total classification error $E(t)$ consists of two components:

(1) The first term $\int_{-\infty}^t f_2(x)dx$: it denotes the probability that an unknown sample is misclassified as a known sample (false negative)

(2) The second term $\int_t^{\infty} f_1(x)dx$: it denotes the probability that a known sample is misclassified as an unknown sample (false positive).

2. Condition for Extremum

Taking the derivative of $E(t)$ with respect to t , we obtain:

$$\frac{dE}{dt} = f_2(t) - f_1(t)$$

Setting the derivative to zero to find the critical point:

$$f_1(T^*) = f_2(T^*)$$

3. Second Derivative Test

Computing the second derivative:

$$\frac{d^2E}{dt^2} = f_2'(t) - f_1'(t)$$

At the intersection point T^* : when $\mu_1 < T^* < \mu_2$, we have $f_1'(T^*) > 0$ (since f_1 is increasing on the right) and $f_2'(T^*) < 0$ (since f_2 is decreasing on the right). Consequently, $\frac{d^2E}{dt^2} \Big|_{t=T^*} > 0$, confirming that T^* is a minimum.

Conclusion : Under the assumption of bimodal Gaussian distributions, the optimal threshold that minimizes the total classification error corresponds to the x-coordinate of the intersection of the two probability density functions.

Theorem 2:

Let the known class follow $N(\mu_1, \sigma_1^2)$ and the unknown class follow $N(\mu_2, \sigma_2^2)$, with probability density functions (PDFs) defined as:

$$f_1(x) = \frac{1}{\sigma_1\sqrt{2\pi}} e^{-\frac{(x-\mu_1)^2}{2\sigma_1^2}}, \quad f_2(x) = \frac{1}{\sigma_2\sqrt{2\pi}} e^{-\frac{(x-\mu_2)^2}{2\sigma_2^2}}.$$

Step 1: Intersection Equation

The intersection of the two distributions satisfies $f_1(x) = f_2(x)$. Simplifying this equality yields:

$$\frac{(x - \mu_1)^2}{\sigma_1^2} - \frac{(x - \mu_2)^2}{\sigma_2^2} = 2 \ln \left(\frac{\sigma_2}{\sigma_1} \right). \quad (1)$$

Step 2: Implicit Function Differentiation

Treating Equation (1) as an implicit function $F(x, \sigma_1) = 0$, we apply the implicit function theorem to compute $\frac{dx}{d\sigma_1}$:

$$\frac{dx}{d\sigma_1} = -\frac{\partial F / \partial \sigma_1}{\partial F / \partial x},$$

where the partial derivatives are:

$$\frac{\partial F}{\partial \sigma_1} = -\frac{2(x - \mu_1)^2}{\sigma_1^3} + \frac{2}{\sigma_1}, \quad \frac{\partial F}{\partial x} = \frac{2(x - \mu_1)}{\sigma_1^2} - \frac{2(x - \mu_2)}{\sigma_2^2}.$$

Step 3: Sensitivity Analysis

As $\sigma_1 \rightarrow 0$: (1) The dominant term in $\partial F / \partial \sigma_1$ is $-\frac{2(x-\mu_1)^2}{\sigma_1^3}$.

(2) The dominant term in $\partial F / \partial x$ is $\frac{2(x-\mu_1)}{\sigma_1^2}$.

Thus,

$$\frac{dx}{d\sigma_1} \approx \frac{\frac{2(x-\mu_1)^2}{\sigma_1^3}}{\frac{2(x-\mu_1)}{\sigma_1^2}} = \frac{x - \mu_1}{\sigma_1}.$$

Conclusion : When σ_1 is extremely small, the magnitude of $\frac{dx}{d\sigma_1}$ scales as $\frac{x-\mu_1}{\sigma_1}$. Even if x is near μ_1 (i.e., the intersection point T^* is close to the known class mean), this derivative remains significant. This demonstrates that the intersection coordinate T^* is highly sensitive to infinitesimal changes in σ_1 . The sensitivity arises from the amplification effect caused by the cubic (σ_1^3) and quadratic (σ_1^2) terms of σ_1 in the denominators of the partial derivatives.

Experiments

Datasets

To comprehensively evaluate the effectiveness of the proposed method, we conduct extensive experimental validation on multiple public datasets. Given that our method does not require source domain data, we first test it on four widely used open-set domain adaptation (OSDA) benchmark datasets: Office-Home (Venkateswara et al. 2017) (65 categories, 4 domains), VisDA-2017 (Peng et al. 2017) (12 categories, cross-domain adaptation from synthetic to real-world scenes), DomainNet (Peng et al. 2019) (345 categories, 6 domains). Furthermore, to further assess the generalization ability of our method, we select 6 publicly available datasets from the Visual Task Adaptation Benchmark (VTAB) for experimentation, including ImageNet (Deng et al. 2009), EuroSAT (Helber et al. 2019), Food101 (Bossard, Guillaumin, and Van Gool 2014), OxfordPets (Parkhi et al. 2012), StanfordCars (Krause et al. 2013) and DTD (Cimpoi et al. 2014). These datasets cover

Setting	ImageNet	DTD	EuroSAT	Food101	OxfordPets	StanfordCars	Office-Home	VisDA-2017	DomainNet
C_{know}	200	20	5	35	20	80	25	6	100
C_{unk}	800	17	5	66	17	116	40	6	245

Table 6: Setting of the Number of Known and Unknown Classes in Different Datasets

Method	VATB-6						DomainNet					AVG	
	ImageNet	DTD	EuroSAT	Food101	OxfordPets	StanfordCars	C	I	P	Q	R		S
MCM-CLIP	61.5	52.7	51.1	74.6	68.2	51.4	75.4	66.3	73.5	38.4	79.2	74.2	63.9
MCM-SigLIP	63.5	68.2	50.2	77.9	75.4	62.6	75.3	67.6	72.4	33	77.2	73.5	66.4
MCM-ALIGN	57.7	62.9	40.8	73.3	63.6	57.2	76.2	68.7	72.2	28.4	80.4	73.3	62.9
UEO-CLIP	56.7	51	44.1	70.1	69.4	50.5	77.4	69.5	75	39.1	81.5	74.9	63.3
UOTA-CLIP	-	-	-	-	-	-	82.4	68.7	77	35.9	85.2	77.3	-
our-CLIP	71.5 ± 0.0	53.2 ± 0.0	51.9 ± 0.0	86.6 ± 0.0	73.4 ± 0.0	55.7 ± 0.0	82.9 ± 0.0	69.1 ± 0.0	79.0 ± 0.0	39.4 ± 0.0	87.3 ± 0.0	79.8 ± 0.0	69.1 ± 0.0
our-SigLIP	69.9 ± 0.0	64.6 ± 0.0	52.3 ± 0.0	84.1 ± 0.0	79.7 ± 0.0	70.7 ± 0.0	79.8 ± 0.0	68.9 ± 0.0	77.2 ± 0.0	35.8 ± 0.0	84.1 ± 0.0	78.8 ± 0.0	70.5 ± 0.0
our-ALIGN	60.7 ± 0.0	68.3 ± 0.0	39.1 ± 0.0	79.6 ± 0.0	66.3 ± 0.0	59.1 ± 0.0	76.6 ± 0.0	68.2 ± 0.0	73.1 ± 0.0	29.1 ± 0.0	82.5 ± 0.0	71.7 ± 0.0	64.5 ± 0.0

Table 7: HOS (%) on VATB and DomainNet (mean ± std) across different methods.

diverse visual tasks, ranging from fine-grained classification to scene recognition, with characteristics such as large category numbers (100-1000 categories), large data scales (tens of thousands to millions of samples), and significant domain differences, providing a comprehensive testing platform for evaluating open-set domain adaptation methods.

In the experiments, the selection criteria for known classes in the four OSDA datasets followed the UOTA (Min et al. 2023) setting to ensure comparability and consistency. For the remaining 6 VATB datasets, we test with varying proportions of unknown classes to enhance the generality and robustness of the experiments, with the specific division of known and unknown classes for each dataset shown in Table 6. Specifically, we sort the class names of each dataset in dictionary order, assigning the first C_{know} classes as known classes, while the rest are considered unknown classes. This diversified testing setup not only validates the adaptability of the method across different data distributions but also comprehensively evaluates its performance on open-set domain adaptation tasks. Additionally, it should be noted that for the 6 VATB datasets, we directly conduct testing on the test set and evaluate performance. The test set partitioning follows the approach of CoOp (Zhou et al. 2022).

Implementation Details. All results are averaged over 5 independent runs with random seeds 1, 2, 3, 4 and 5. Since our method involves inference only and requires no training, the variance is negligible (effectively near zero). Experiments were performed on an Intel Xeon Gold 6442Y CPU, a Tesla L40 GPU, and 512 GB of RAM running Ubuntu 18.04. The software environment consists of Python 3.8.20 and PyTorch 2.0.1. Unless stated otherwise, we used a batch size of 32 and a temperature $\tau = 0.8$. Since our method is training-free, no learning-rate hyperparameter is required.

Baselines

To the best of our knowledge, the proposed Source-Free open-set domain adaptation (SF-OSDA) method, which requires neither source domain data nor training, has not been

explored in existing research. Therefore, we select the following three categories of baseline methods for comparison to ensure the comprehensiveness and fairness of the evaluation:

- The VLM-based zero-shot out-of-distribution detection method MCM (Ming et al. 2022). In our experiments, as a baseline, we adopt the commonly used and relatively stable approach in OSDA by using the mean score of all test samples as the default threshold, since the original paper does not specify a concrete thresholding strategy.
- Unsupervised open-set domain adaptation (OSDA) methods jointly train on labeled source and unlabeled target domains, including USD (Jahan and Savakis 2024), UniOT (Chang et al. 2022), OSMDA (Liu et al. 2025) and GLC (Qu et al. 2023). During training, these methods treat all labeled source-domain classes as known and regard any target-domain classes outside this set as unknown.
- Source-free unsupervised OSDA methods use a model trained on the labeled source domain as a reference for unsupervised training on the unlabeled target domain, including LAED (Qu et al. 2024), DIFO (Tang et al. 2024), Co-learn++ (Zhang, Shen, and Foo 2025), COSDA (Wang et al. 2025), UPUK (Wan et al. 2024), COCA (Liu and Zhou 2024), COSDA (Wang et al. 2025) and DIFO (Tang et al. 2024). These methods designate the classes encountered during source-domain training as known and treat all other target-domain classes as unknown.
- Target-only unsupervised open-set domain adaptation methods, such as UOTA (Min et al. 2023) and UEO (Liang et al. 2024), perform training exclusively on the unlabeled target-domain data. They define a predefined set of known classes and treat all other classes in the target data as unknown.

Through the comparison of these three categories of baseline methods, we can comprehensively assess the perfor-

Method	Art	Clipart	Product	Real	Visda	ImageNet	DTD	EuroSAT	Food101	OxfordPets	StanfordCars	↓ AVG
CLIP	0.40	0.55	0.65	0.53	0.33	0.39	0.29	0.80	0.32	0.76	0.62	0.51
CLIP w/ SUFF	0.15	0.35	0.28	0.17	0.00	0.24	0.24	0.80	0.15	0.65	0.58	0.33 (↓ 0.18)
Siglip	0.55	0.82	0.75	0.57	0.50	0.46	0.53	0.40	0.36	0.76	0.84	0.59
Siglip w/ SUFF	0.20	0.38	0.17	0.20	0.33	0.23	0.12	0.60	0.08	0.35	0.53	0.29 (↓ 0.30)
ALIGN	0.42	0.65	0.60	0.47	0.50	0.41	0.41	0.80	0.33	0.76	0.72	0.55
ALIGN w/ SUFF	0.12	0.15	0.15	0.12	0.17	0.26	0.06	0.40	0.15	0.53	0.54	0.24 (↓ 0.31)

Table 8: AR@1 before and after applying the SUFF module on VATB-6, Office-Home (Art, Clipart, Product, Real), and VisDA-2017 datasets.

mance of the proposed method in different scenarios and validate its unique advantages in the absence of source domain data and training conditions.

Additionally, to facilitate performance comparison with other OSDA methods, we use the commonly adopted HOS metric, which is the harmonic mean of the average accuracy for known classes and the accuracy for unknown classes. The calculation formula is as follows:

$$HOS = \frac{2 \cdot Acc_{\text{known}} \cdot Acc_{\text{unknown}}}{Acc_{\text{known}} + Acc_{\text{unknown}}}, \quad (18)$$

where Acc_{known} represents the average accuracy of known classes, and Acc_{unknown} denotes the accuracy of unknown class recognition. This metric reflects the overall performance of the model on both known and unknown classes, balancing the recognition ability for known classes and the detection ability for unknown classes. Therefore, HOS provides an effective standard for evaluating OSDA methods.

Overall Performance

In this section, we present the detailed data for the results shown in Table 2 of the main text. To ensure a fair comparison, both UEO and MCM use the same threshold-selection method in Table 2—namely, the average of all sample scores, which is a common and stable choice. The full results are listed in Table 7.

From the detailed results in Table 7, our method delivers significant improvements over the VLM-based MCM on every dataset. In particular, on ImageNet under CLIP, we see up to a 10 % gain, and even on DTD—where CLIP’s zero-shot performance is relatively weak—we achieve a 0.5 % uplift. This demonstrates our approach’s robustness to noise in VLM predictions, maintaining stability even when zero-shot accuracy is low. Moreover, on the most challenging domain-adaptation dataset, DomainNet, we outperform the previous training-intensive SOTA method UOTA across all domains. These findings confirm the effectiveness of our lightweight inference strategy for VLMs in OSDA scenarios, achieving SOTA performance without any additional training.

Performance Comparison: VLM-OpenXpert vs. ChatGPT-4o and 4o-mini

To evaluate the ability of our method to reject unknown classes compared to the latest cross-modal large language models, we conducted experiments on three datasets of varying scales: the Real domain of OfficeHome, the Clipart domain of DomainNet, and Flowers102 (Nilsback and

Zisserman 2008). We crafted refined prompts to guide ChatGPT-4o and 4o-mini in determining whether an image belongs to a given category set—if so, they classify it. Their performance is then compared with our lightweight model, VLM-OpenXpert.

Method	Officehome-R	DomainNet-C	Flowers102	AVG
ChatGPT-4o	89.2	55.0	53.5	65.9
ChatGPT-4o-mini	84.8	55.0	52.7	64.1
our-CLIP (Vit-L/14)	89.5 ± 0.0	83.2 ± 0.0	70.2 ± 0.0	81.0 ± 0.0
our-CLIP (Vit-B/16)	85.4 ± 0.0	75.6 ± 0.0	68.8 ± 0.0	76.6 ± 0.0

Table 9: HOS (%) Performance Comparison with Cross-Modal LLMs (ChatGPT-4o and 4o-mini)

We provided ChatGPT with the prompt: "Given the image, determine if the main object belongs to one of these categories: CLASS NAMES. If yes, reply with the category name. Otherwise, reply "unknown". Here, CLASS NAMES is replaced with the list of known categories from the dataset. Based on its responses, we performed text matching to evaluate its ability to reject unknown classes and recognize known ones. As shown in Table 9, on the small-scale Office-Home Real domain (with only 25 known classes), ChatGPT-4o achieved performance comparable to our ViT-L/14-based model. However, as the dataset scale and number of categories increased—for example, DomainNet-C (100 classes) and Flowers102 (65 classes)—ChatGPT’s performance dropped sharply and fell far behind our method. This decline is mainly due to ChatGPT being designed as a general-purpose vision-language model, not specifically for classification tasks. These results highlight that despite the impressive capabilities of large cross-modal models, developing lightweight VLMs remains highly valuable for fundamental tasks like image classification.

Ablation Study

This section provides additional ablation study experiments that are not detailed in the main text, including the exact numerical values of some tables and figures, as well as ablation experiments omitted due to space constraints. A more comprehensive dataset and ablation results are presented in this subsection.

Analysis of the SAA Phenomenon. Since vision-language models (VLMs) perform classification by measuring similarity between image and text embeddings, the predicted label distribution of unknown samples

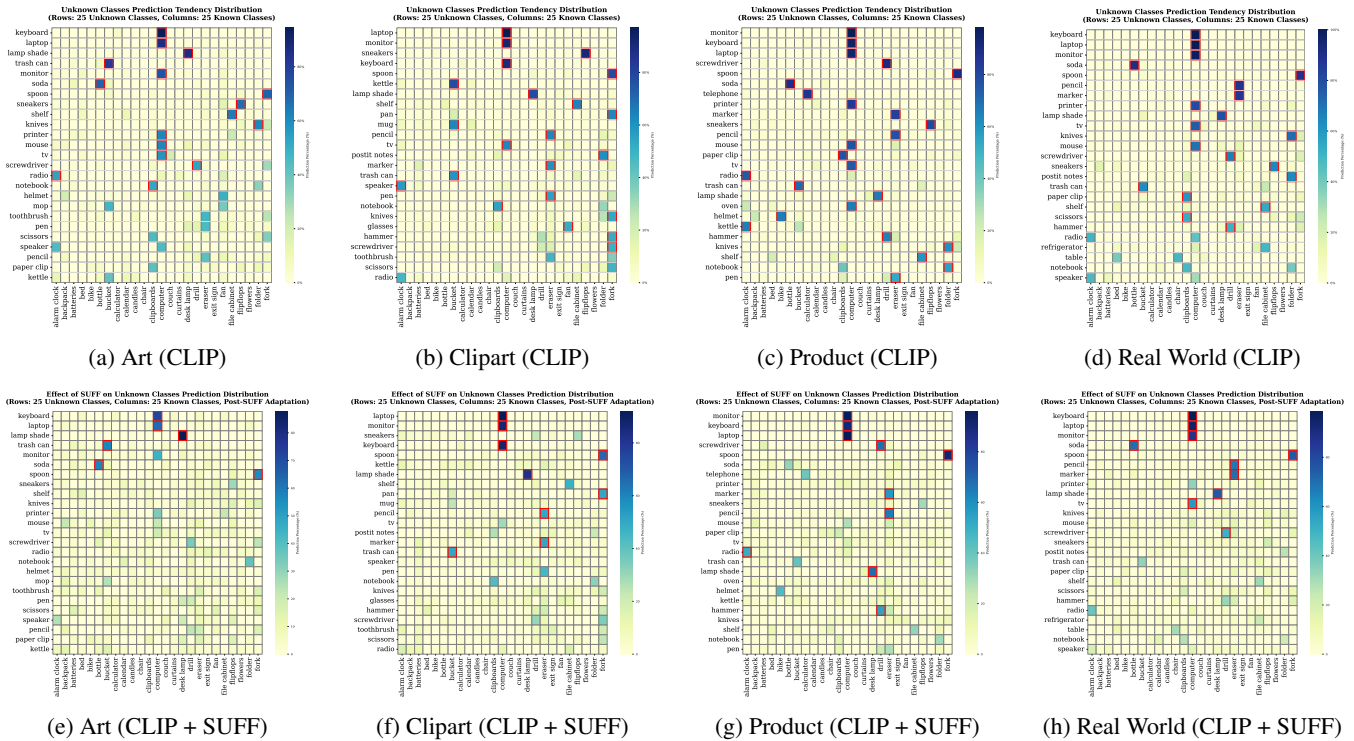


Figure 7: Samples of the 25 classes with the strongest tendency towards known classes from the four domains of the Office-Home dataset. The figure shows the changes in classification results for known classes between the original CLIP features and the features filtered by the SUFF module. Rows represent unknown classes, columns represent known classes, and the darker the cell, the more samples from the corresponding unknown class are classified into the corresponding known class.

Method	w/ SUFF	ImageNet	OfficeHome				VisDA	AVG
			Art	Clipart	Product	Real		
our-CLIP	×	61.6	61.9	59.9	46.4	52.8	83.8	61.1
	✓	69.6	80.2	72.1	85.7	85.0	89.0	80.3
our-SigLIP	×	52.6	53.0	42.8	48.7	47.4	55.6	50.0
	✓	64.1	67.7	47.8	68.8	66.4	69.5	64.0
ALIGN	×	57.1	78.4	73.1	89.9	79.9	75.1	75.6
	✓	59.6	84.4	80.7	90.5	90.3	86.1	81.9

Table 10: Impact of the SUFF module on HOS (%) for different VLM models under a fixed threshold function.

Method	w/ SUFF	ImageNet	OfficeHome				VisDA	AVG
			Art	Clipart	Product	Real		
our-CLIP	×	62.1	74.7	69.3	72.7	77.4	86.3	73.7
	✓	70.8	79.9	73.1	86.2	85.2	89.0	80.7
our-SigLIP	×	60.9	76.5	65.0	70.1	73.4	75.8	70.3
	✓	66.5	80.6	67.8	80.8	81.3	80.3	76.2
ALIGN	×	52.6	81.7	77.0	90.6	84.7	75.8	77.1
	✓	64.1	84.5	82.2	90.9	90.9	80.3	82.1

Table 11: Impact of SUFF on HOS (%) for different VLM models using a K-means threshold function.

Method	w/ SUFF	ImageNet	OfficeHome				VisDA	AVG
			Art	Clipart	Product	Real		
our-CLIP	×	63.3	76.5	71.7	82.1	82.8	87.8	77.3
	✓	71.3	78.2	74.0	86.8	85.7	89.0	80.8
our-SigLIP	×	67.2	83.7	80.8	89.2	88.2	87.4	82.7
	✓	69.9	85.8	80.4	89.4	88.9	88.1	83.7
ALIGN	×	59.4	81.4	81.1	90.8	88.9	86.1	81.3
	✓	60.7	85.0	83.2	90.9	91.3	87.3	83.1

Table 12: Impact of SUFF on HOS(%) for different VLM models using our BGAT threshold function.

reflects their semantic proximity to known categories.

In an ideal open-set setting, if the unknown classes are semantically unrelated to all known classes, their predictions should be uniformly scattered across the known categories due to the absence of strong similarity signals. However, when certain unknown classes are semantically close to specific known classes, VLMs tend to consistently misclassify them into those nearby categories, forming a phenomenon we refer to as *semantic affinity anchoring*.

To quantitatively assess the prevalence of this Semantic Affinity Anchoring (SAA) effect in existing benchmarks, we propose a simple yet effective metric: **Anchor Rate at Top-1 (AR@1)**. This metric measures, at the dataset level, the proportion of unknown classes whose samples are consistently mapped to a particular known class.

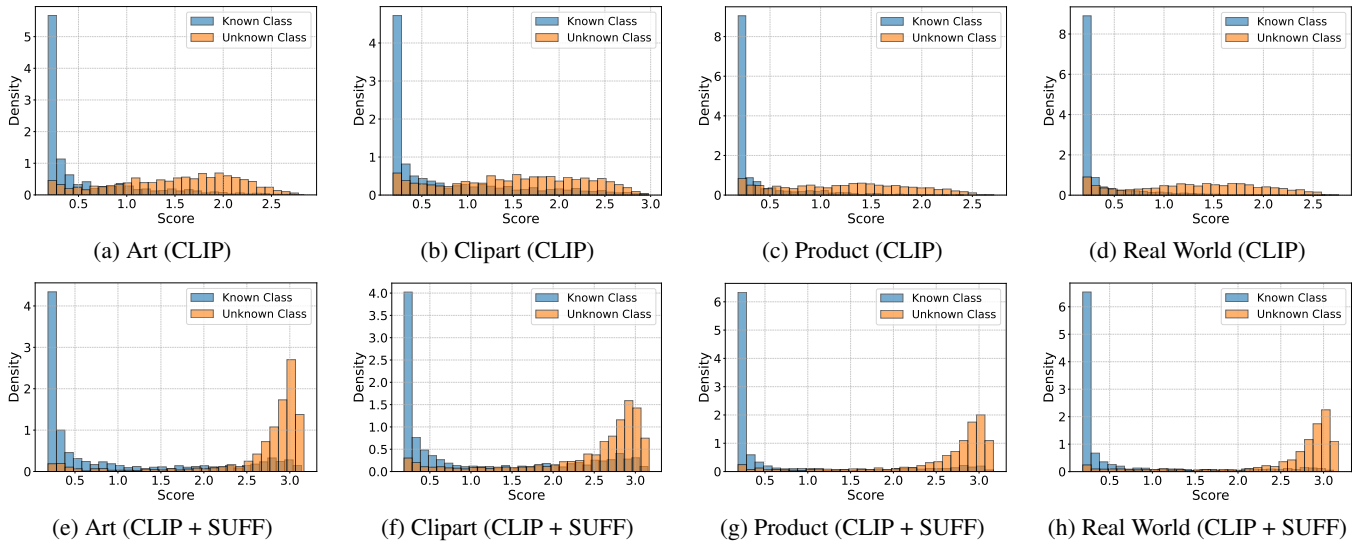


Figure 8: Changes in the entropy of samples from the four domains of the Office-Home dataset before and after processing by the SUFF module. The first row shows the entropy computed from the original CLIP features, while the second row displays the entropy of the samples after filtering by the SUFF module.

Formally, we define the following:

- C be the known-class set, $|C| = K$;
- U the unknown classes that actually occur in the test set, $|U| = M$;
- N_u the number of test samples belonging to the unknown class $u \in U$;
- $\hat{y}_i \in C$ the VLM’s top-1 prediction for sample x_i .

Method	Threshold	ImageNet	OfficeHome				VisDA	AVG
			Art	Clipart	Product	Real		
CLIP	Fixed	61.6	61.9	59.9	46.4	52.8	83.8	61.1
	Mean	61.9	76.4	69.6	76.1	80.1	86.8	75.1
	K-means	62.1	74.7	69.3	72.7	77.4	86.3	73.8
	GMM-int	63.2	57.5	54.8	58.7	57.7	72.1	60.7
	BGAT	63.3	76.5	71.7	82.1	82.8	87.8	77.4

Table 13: Comparison of HOS (%) for the CLIP model under different threshold functions.

For each unknown class u , we build a prediction distribution over known classes as:

$$p_{u,c} = \frac{1}{N_u} \sum_{i: y_i=u} \mathbf{1}[\hat{y}_i = c], \quad \sum_{c \in C} p_{u,c} = 1.$$

Given a threshold $\tau \in (0, 1)$, the Anchor Rate at Top-1 is:

$$\text{AR@1}(\tau) = \frac{1}{M} \sum_{u \in U} \mathbf{1}[\max_{c \in C} p_{u,c} \geq \tau].$$

The AR@1 metric possesses the following key properties:

- **Dataset-level metric:** used to evaluate the proportion of unknown classes anchored to known classes in a dataset.
- **Threshold-controlled:** larger τ makes anchoring harder to satisfy. In this paper, we set $\tau = 0.5$ by default.

- **Range:** $\text{AR@1} \in [0, 1]$; A value closer to 0 indicates fewer unknown classes are anchored, while a value closer to 1 indicates more anchoring. A value of 1 means all unknown classes are anchored to specific known classes, whereas 0 means none exhibit significant anchoring.

As reported in Table 8, all three VLMs demonstrate a pronounced semantic affinity anchoring (SAA) effect across all datasets. It can be observed that, across all three VLM models, the average AR@1 scores exceed 0.5, indicating that over 50% of the unknown classes have more than half of their samples anchored to the same known class. This demonstrates that the Semantic Affinity Anchoring (SAA) phenomenon is prevalent in current benchmark datasets.

Method	Threshold	ImageNet	OfficeHome				VisDA	AVG
			Art	Clipart	Product	Real		
CLIP w/ SUFF	Fixed	69.6	80.2	72.1	85.7	85.0	89.0	80.3
	Mean	70.2	80.4	72.3	84.2	84.7	88.3	80.0
	K-means	70.8	79.9	73.1	86.2	85.2	89.0	80.7
	GMM-int	69.3	76.6	58.8	53.7	57.4	88.6	67.4
	BGAT	71.3	78.2	74.0	86.8	85.7	89.0	80.8

Table 14: Comparison of HOS (%) for the CLIP model with SUFF under different threshold functions.

Effectiveness of SUFF. The SUFF module is designed to address the difficulty of detecting certain known classes caused by semantic affinity anchoring (SAA). To fully assess its impact, we evaluate its performance in two ways. First, as shown in Table 8, adding SUFF to CLIP, SigLIP, and ALIGN reduces AR1 by 0.28, 30.0, and 0.31, respectively, demonstrating its effectiveness at alleviating SAA. Second, examining overall performance (Tables 10, 11, 12), SUFF significantly boosts HOS across all threshold functions—most notably by 19.2%, 14.0%, and 6.3% under the simple Fixed threshold—and also delivers substantial gains

under the K-meas and our BGAT thresholds. These results confirm that SUFF markedly improves model performance by mitigating the SAA effect.

Method	Threshold	ImageNet	OfficeHome				VisDA	AVG
			Art	Clipart	Product	Real		
SigLIP	Fixed	52.6	53.0	42.8	48.7	47.4	55.6	50.0
	Mean	63.2	80.5	72.5	76.5	78.9	81.5	75.5
	K-means	60.9	76.5	65.0	70.1	73.4	75.8	70.3
	GMM-int	37.3	68.5	69.6	77.2	80.7	74.7	68.0
	BGAT	67.2	83.7	80.8	89.2	88.2	87.4	82.7

Table 15: Comparison of HOS (%) for the SigLIP model under different threshold functions.

Effectiveness of BGAT. We compare our BGAT adaptive-threshold module against four established methods: a fixed threshold at half the maximum score (Fixed) (Yu, Irie, and Aizawa 2025), the mean of all sample scores (Mean) (Bucci, Loghmani, and Tommasi 2020), k-means clustering (K-Means) (Liang, Hu, and Feng 2020), and the intersection point of two Gaussian densities (GMM-Int) (He, Wang, and Zhang 2025). We conduct evaluation across six diverse tasks—ImageNet, four domains from OfficeHome (Art, Clipart, Product, Real), and VisDA-2017—and test three different VLM models to comprehensively validate the effectiveness of our thresholding function.

Method	Threshold	ImageNet	OfficeHome				VisDA	AVG
			Art	Clipart	Product	Real		
SigLIP w/ SUFF	Fixed	64.1	67.7	47.8	68.8	66.4	69.5	64.0
	Mean	66.7	79.2	70.9	77.7	78.8	81.5	75.8
	K-means	66.5	80.6	67.8	80.8	81.3	80.3	76.2
	GMM-int	44.8	79.4	80.9	84.7	84.1	80.8	75.8
	BGAT	69.9	85.8	80.4	89.4	88.9	88.1	83.7

Table 16: Comparison of HOS (%) for the SigLIP model with SUFF under different threshold functions.

As shown in Tables 13-18, our BGAT module consistently delivers the best performance across all VLM backbones. In particular, on the raw scores derived from pre-SUFF features, BGAT outperforms the four baseline thresholding methods on SigLIP by 32.7%, 7.2%, 12.4%, and 14.7%, respectively. This gap arises because the original VLM score distributions exhibit poor class separability and are highly sensitive to threshold choice. Even after applying the SUFF module—which substantially reduces score sensitivity—BGAT still surpasses the competing methods by 19.7%, 7.9%, 7.5%, and 7.9%. These results confirm that BGAT provides a more robust and reliable threshold selection across a wide range of score distributions.

Effectiveness of Box-Cox. The BGAT module consists of a Box-Cox transformation and a Gaussian mixture model. The Box-Cox transformation aims to correct the skewness of the score distribution, making it more Gaussian-like and improving the accuracy of threshold estimation. To validate its effectiveness, we conduct experiments on all four domains of Office-Home, comparing the performance of CLIP, SigLIP, and ALIGN with and without the Box-Cox transformation.

Method	Threshold	ImageNet	OfficeHome				VisDA	AVG
			Art	Clipart	Product	Real		
ALIGN	Fixed	57.1	78.4	73.1	89.9	79.9	75.1	75.6
	Mean	59.3	82.6	77.9	90.0	86.1	83.0	79.8
	K-means	52.6	81.7	77.0	90.6	84.7	75.8	77.1
	GMM-int	59.0	57.2	66.4	52.9	67.3	66.2	61.5
	BGAT	59.4	81.4	81.1	90.8	88.9	86.1	81.3

Table 17: Comparison of HOS (%) for the ALIGN model under different threshold functions.

Method	Threshold	ImageNet	OfficeHome				VisDA	AVG
			Art	Clipart	Product	Real		
ALIGN w/ SUFF	Fixed	59.6	84.4	80.7	90.5	90.3	86.1	81.9
	Mean	61.4	84.3	81.3	91.0	87.7	86.2	82.0
	K-means	64.1	84.5	82.2	90.9	90.9	80.3	82.1
	GMM-int	53.1	59.8	67.4	86.6	63.7	66.3	66.1
	BGAT	60.7	85.0	83.2	90.9	91.3	87.3	83.1

Table 18: Comparison of HOS (%) for the ALIGN model with SUFF under different threshold functions.

VLM	Box-Cox	Office-Home				VisDA	AVG
		Art	Clipart	Product	Real		
SigLIP	no	81.5	72.9	80.7	80.9	83.6	79.9
	yes	85.8	80.4	89.4	88.9	88.1	86.5
ALIGN	no	84.4	82.0	91.3	89.1	86.9	86.7
	yes	85.0	83.2	90.9	91.3	87.3	87.5
CLIP	no	77.6	73.9	85.8	84.7	88.6	82.1
	yes	78.2	74.0	86.8	85.7	89.0	82.7

Table 19: HOS (%) before and after applying the Box-Cox transformation across different VLMs.

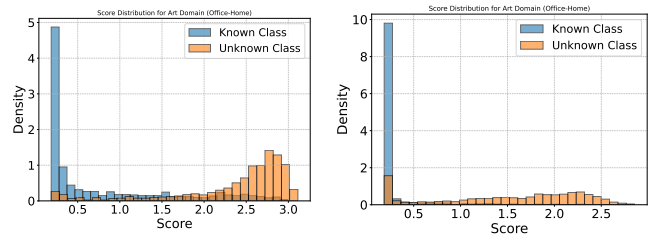


Figure 9: Entropy distribution of sample scores from CLIP and SigLIP on the Art domain of the Office-Home dataset.

As shown in Table 19, the Box-Cox transformation is highly effective for the SigLIP model, yielding an average performance gain of 6.6% across the four domains. In contrast, CLIP and ALIGN achieve smaller improvements of 0.6% and 0.8%, respectively, with an overall average gain of 2.67%. This demonstrates the effectiveness of the proposed Box-Cox transformation. Moreover, the larger gain observed in SigLIP can be attributed to its score distribution: as shown in Figure 9, the known-class scores (measured by entropy) in SigLIP exhibit significantly higher skewness than those in CLIP on the same dataset.

Runtime Analysis and Comparison

Runtime Profiling of Inference and SUFF (SVD) Module.

Our VLM-OpenXpert framework adds two inference modules that introduce a modest overhead to the base model’s runtime. To quantify this overhead, we profiled the time spent in each component on the training splits of the Real domain in Office-Home, the VisDA-2017 benchmark, and all domains of DomainNet. All measurements were taken under identical hardware conditions: an Intel Xeon Gold 6442Y CPU and a Tesla L40 GPU.

We partitioned the inference process into three components: (1) VLM feature encoding; (2) the two SVD decompositions in SUFF; and (3) all other feature operations and processing, including BGAT. As shown in Table 20, roughly 97.5% of runtime is spent on VLM feature encoding, SVD takes under 0.5%, and the remaining operations (including BGAT) account for only about 2%. This confirms that our method adds minimal computational overhead to the inference process.

Adaptation Time Comparison with Trainable SF-OSDA Methods. We conduct this experiment to evaluate the adaptation time advantage of our method over trainable SF-OSDA approaches. Specifically, we compare with two representative methods: SHOT, a widely used SF-OSDA method, and UEO, a target-only open-set adaptation method based on the same VLM (CLIP). For a fair comparison, we only measure the adaptation time on the target domain, excluding source domain training. We also ensure that the image encoder is the same across methods, and that our method and UEO use the same VLM.

As shown in Table 21, our method achieves significantly faster adaptation compared to other approaches. Specifically, it requires only 1.8% of SHOT’s adaptation time on the target domain. Even compared to UEO, which benefits from prompt learning and has relatively fast training, our method takes only 4.2% of its time. These results clearly demonstrate the substantial speed advantage of our approach over previous training-intensive methods.

Impact of Varying Unknown-Class Proportions. To assess the effect of varying unknown-class ratios, we used the Office-Home dataset across its four domains. Since this factor is seldom studied, we reproduced two representative open-source baselines—SHOT and UEO—and adopted the same CLIP backbone as UEO.

Office-Home comprises 65 classes. We evaluated five scenarios with 60, 50, 40, 30, and 25 unknown classes. Thanks to our plug-and-play design, we also measured how integrat-

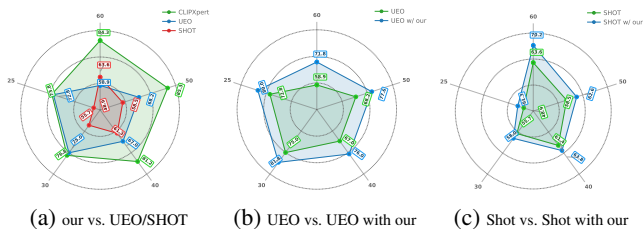


Figure 10: Performance vs. Number of Unknown Classes.

ing our method into SHOT and UEO affects their performance. (For UEO as a baseline, thresholds were set to the mean score.)

As shown in Figure 10, our method outperforms SHOT and UEO at all ratios, with peak gains of 25.5% and 20.7%, respectively. When our method is applied to extend SHOT and UEO, their performance further improves by up to 12.95% under varying ratios. These results confirm the robustness of our approach to changes in the number of unknown classes.

	Office-Home(R)	VisDA-2017	DomainNet
Sample counts	4375	55388	596006
Total time	20.18	140.75	1455.82
CLIP encoding time	19.82	136.29	1438.47
SVD time	0.11 (0.5%)	0.18 (0.1%)	2.357 (0.2%)
other	0.36 (1.8%)	4.46 (3.2%)	17.35 (1.2%)

Table 20: Detailed time consumption of each inference component

Method	OfficeHome				Visda-2017	AVG
	Art	cliipart	product	real		
our-CLIP	6.9	11.0	11.1	20.2	143.0	38.4
SHOT	325.1	553.6	566.3	811.2	8684.6	2188.2
UEO-CLIP	285.9	356.9	367.0	347.1	3192.0	909.8

Table 21: Comparison of adaptation time across different methods

Statistical Significance and Robustness

Ablation Study Significance Tests. As our method is training-free and performs direct inference on the test set, its performance is minimally affected by random seeds, with standard deviations nearly zero. We therefore treat datasets as the paired unit for significance analysis of the core ablation results. Using CLIP as the backbone, we evaluate across 11 tasks, including the four domains of OfficeHome, the VisDA test domain, and six VTAB datasets. We compare our proposed BGAT against direct CLIP-based scoring and four alternative thresholding strategies to demonstrate the effectiveness of BGAT. Additionally, we compare results with and without SUFF (using BGAT as the thresholding method) to validate the contribution of the SUFF module.

For each comparison, we compute per-dataset HOS differences and perform a *paired t*-test, reporting the mean differ-

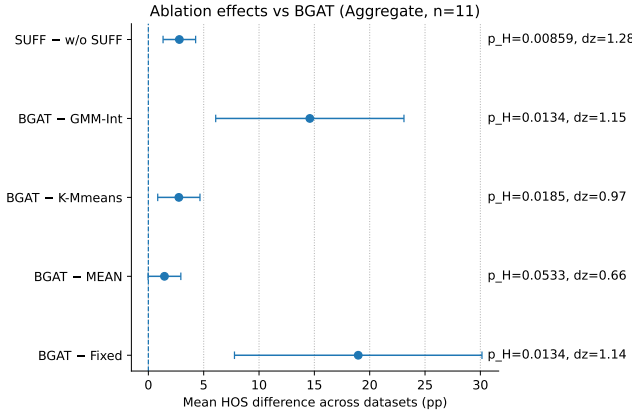


Figure 11: Aggregate ablation effects across 11 datasets (paired by dataset). Points denote mean HOS differences (pp) with 95% confidence intervals; the dashed line marks no gain (0). Holm–Bonferroni–adjusted p -values and effect sizes (Cohen’s d_z) are annotated.

Comparison	Mean diff(pp)	95% CI (pp)	p_t	p_{Holm}	d_z	p_{Wilcox}
BGAT vs Fixed	18.96	[7.78, 30.15]	0.0036	0.0134	1.14	0.005
BGAT vs Mean	1.45	[-0.03, 2.93]	0.0533	0.0533	0.66	0.0674
BGAT vs K-Means	2.75	[0.85, 4.66]	0.0093	0.0185	0.97	0.001
BGAT vs GMM-Int	14.59	[6.08, 23.10]	0.0034	0.0134	1.15	0.0049
SUFF vs w/o SUFF	2.8	[1.33, 4.27]	0.0017	0.0086	1.28	0.001

Table 22: Paired two-sided t -tests across 11 datasets ($n=11$). Entries are mean HOS differences in percentage points (pp); 95% CIs are t -based confidence intervals for the mean difference. p_t are unadjusted; p_{Holm} are Holm–Bonferroni adjusted across the five planned comparisons; p_{Wilcox} are unadjusted two-sided signed-rank p -values as a robustness check. Cohen’s $d_z = \bar{\Delta}/s_{\Delta}$.

ence, the t -based 95% confidence interval (CI), and Holm–Bonferroni adjusted p -values; nonparametric Wilcoxon results point in the same direction. Aggregate statistics are in Table 22: BGAT vs. Fixed shows +18.96 pp (95% CI [7.78, 30.15], $p_H = 0.0134$); BGAT vs. K-Means +2.75 pp ([0.85, 4.66], $p_H = 0.0185$); BGAT vs. GMM-Int +14.59 pp ([6.08, 23.10], $p_H = 0.0134$); BGAT vs. MEAN shows a +1.45 pp positive, near-threshold trend at $\alpha = 0.05$; adding SUFF on top of BGAT yields a significant +2.80 pp ([1.33, 4.27], $p_H = 0.0086$). The forest plot (Figure 11) highlights comparisons whose CIs lie entirely to the right of 0; effect sizes (Cohen’s d_z) are generally large (Table B.1), indicating not only statistical but also practically meaningful gains.

Case Study

To analyze the tendency of removing certain unknown classes on the known classes, we visualize the distribution of the top 25 classes with the strongest tendency in the Office-Home dataset across four domains before and after filtering by the SUFF module. We also compare the change in entropy of all samples before and after filtering by the SUFF module.

Algorithm 1: VLM-OpenXpert Algorithm

Require: Unlabeled target dataset $D_t = \{x_i^t\}_{i=1}^{N_t}$, known class label set $L_t = \{l_1, \dots, l_C\}$ where l_c denotes the c -th class, along with an image encoder E and a text encoder G .

Ensure: Final classification predictions for D_t

- 1: Extract features: $X_{all} \leftarrow E(D_t)$, $X_{text} \leftarrow G(L_t)$ \triangleright (Via Eq. 3)
- 2: Obtain initial predictions: $(\hat{y}, \text{Scores}) \leftarrow \text{Classify}(X_{all}, X_{text})$ \triangleright (Via Eqs. 1 and 4)
- 3: Normalize scores: $\text{Scores} \leftarrow \text{Box-CoxTransform}(\text{Scores})$ \triangleright (Via Eqs. ?? and 5)
- 4: Estimate parameters: $\mu_{know}, \mu_{unk}, T_{init}^* \leftarrow \text{fit GMM}(\text{Scores})$ \triangleright (Using Eq. 7)
- 5: Revert transformation: $(\mu_{know}, \mu_{unk}, T_{init}^*) \leftarrow \text{InverseBoxCox}(\cdot)$ \triangleright (Via Eq. 8)
- 6: Partition features:
 - $X_{know} \leftarrow \{x \in X_{all} \mid \text{Score}(x) < \frac{1}{2}(\mu_{know} + T_{init}^*)\}$
 - $X_{unk} \leftarrow \{x \in X_{all} \mid \text{Score}(x) > \frac{1}{2}(\mu_{unk} + T_{init}^*)\}$
- 7: Subspace decomposition:
 - $Z_{know} \leftarrow \text{SVD}(X_{know})$, $Z_{unk} \leftarrow \text{SVD}(X_{unk})$ \triangleright (Via Eqs. 9, 10)
 - $X_{all}^{know} \leftarrow \text{Project}(X_{all}, Z_{know})$ \triangleright (Via Eq. 12)
 - $X_{all}^{unk} \leftarrow \text{Project}(X_{all}, Z_{unk})$ \triangleright (Via Eq. 13)
- 8: Compute feature ratio: $\alpha(X_{all}) \leftarrow \frac{\|X_{all}^{unk}\|}{\|X_{all}\|}$ \triangleright (Via Eq. 16)
- 9: Filter features: $X_{all}^* \leftarrow \text{FeatureFilter}(X_{all}, \alpha(X_{all}))$ \triangleright (Via Eq. 17)
- 10: Recalculate scores and estimate the threshold T^* :
 - $\text{Scores}^* \leftarrow \text{RecomputeScores}(X_{all}^*, X_{text})$
 - Execute steps 3, 4, and 5 again using Scores^* to obtain the estimated final threshold T^* .
- 11: Generate final predictions: $\text{Predictions} \leftarrow \text{Threshold-based Classify}(\text{Scores}^*, T^*, \hat{y})$ \triangleright (Via Eq. 2) **return** Predictions

As shown in Figure 7, each cell represents the distribution of predictions for all samples of an unknown class in one row, with each column indicating the distribution of unknown classes predicted as a specific known class. The darker the cell color, the more samples from the unknown class are classified into the corresponding known class. As shown in the first row of Figure 7, it is evident that in the original CLIP predictions, many unknown classes exhibit a strong tendency toward known classes, causing these samples to have scores very close to known classes. This results in difficulty distinguishing these samples during unknown class detection. As shown in the second row of Figure 7, after filtering by the SUFF module, the number of unknown classes with significant tendencies is notably reduced, allowing these hard-to-detect unknown class samples to be separated from the known classes.

Additionally, as shown in the first row of Figure 8, the entropy of unknown classes computed from the original CLIP features is spread across different score ranges and signif-

icantly overlaps with that of the known classes. However, as shown in the second row of Figure 8, after filtering by the SUFF module, the entropy of the unknown classes shifts significantly toward the maximum value, greatly enhancing the separability between known and unknown classes. Furthermore, it can be observed that the entropy of the known classes does not shift to the right during the feature filtering process, indicating that the SUFF module does not destroy the separability of known class features while filtering unknown class features.

Algorithm Details and Pseudocode

In this section, we provide the detailed pseudocode of VLM-OpenXpert. Our method aims to detect unknown samples and classify known-class samples in an unlabeled target dataset without requiring any source-domain data or additional training. The approach consists of the following key steps: (1) We leverage a VLM (e.g., CLIP) as an encoder to perform zero-shot classification, obtaining the initial classification results for known classes and computing sample scores based on these results; (2) The proposed BGAT module estimates the distribution of sample scores and derives the estimated mean scores for known and unknown classes, along with an initial threshold; (3) Based on these estimates, we perform an initial selection of samples and apply the proposed SUFF module to filter out unknown-class features; (4) We then recompute sample scores using the filtered features and re-estimate the final threshold via the BGAT module; (5) Finally, we classify all samples using the refined scores, the final threshold, and the initial classification results. The full procedure is detailed in Algorithm 1.